IEEE Access
Multidisciplinary ⋮ Rapid Review ⋮ Open Access Journal

Received 11 May 2024, accepted 25 May 2024, date of publication 28 May 2024, date of current version 28 June 2024.

Digital Object Identifier 10.1109/ACCESS.2024.3406672

RESEARCH ARTICLE

Effective Design of an Array of Coupling Slots With a Reflection-Canceling Wall for a Parallel-Plate Slot Array Antenna

TIANYU WANG, TAKASHI TOMURA, (Member, IEEE), AND JIRO HIROKAWA, (Fellow, IEEE)
Department of Electrical and Electronic Engineering, Tokyo Institute of Technology, Tokyo 152-8552, Japan
Corresponding author: Takashi Tomura (tomura@ee.e.titech.ac.jp)

ABSTRACT This paper presents an effective design of an array of coupling slots with reflection-canceling walls for uniform excitation of a parallel-plate slot array antenna panel. The coupling slot array is analyzed by Galerkin's method of moments (MoM) for the fast design by simplifying to use only uniform current on the reflection-canceling walls. It takes only 20 seconds to analyze an array of 14 coupling slots by MoM by a laptop PC having a 16-core Intel Core i7 CPU with 2.60GHz base frequency and 16 GB RAM while it takes 4 hours by HFSS. The values of parameters of each coupling slot by MoM are replaced with those by HFSS having the equal scattering matrix components.

INDEX TERMS Planar slotted waveguide array, parallel-plate antenna, method of moments (MoM), equivalent relationship.

I. INTRODUCTION

Nowadays, parallel-plate slot array antennas are attractive candidates especially in centimeter- and millimeter-wave band due to their intrinsic advantages of high gain, high antenna radiation efficiency, low losses, compact structure, and high-power capability. These characteristics make them suitable for various applications [1], [2], [3]. Compared to the commonly used planar slotted array antenna configuration consists of array of juxtaposed waveguides under single-mode operation with proper feeding circuit beneath [4], [5] or distribution networks at the same layer [6], [7], the suppression of the inner sidewalls eliminates the necessity of a minimum distance between radiating elements, which makes the slot array deign more flexible. Also, it avoids the requirement of a perfect electrical contact between the top plate consisting of radiating slots and the bottom grooved feed surface, which facilitates the manufacturing process and suitable for mass production.

General-purpose commercial software such as CST or HFSS with high accuracy have been widely used in slotted array antenna design due to the drastically improvement of computer performance [8], [9]. However, parallel-plate antenna analysis needs to treat the mutual coupling among the slots carefully and a calculation by software is time consuming due to many unknowns. Analysis by the method of moments (MoM) requires much less unknowns and turns out to be advantageous for a large-scale array fast design [10], [11], [12]. Usually, the dyadic Green's function needed for the MoM procedure could be obtained in a closed form benefit from the regular shape of the splitting segments [13], [14], [15], which also increases the calculation speed.

In this paper, the feeder waveguide for a parallel-plate antenna with reflection-canceling inductive walls inside is designed by MoM. A similar antenna configuration with circular polarization and end-feed scheme is proposed in [16]. The feeding network is designed by HFSS and the in-phase condition is guaranteed by an iterative algorithm. However, the internal mutual coupling among elements inside the feeding waveguide is not taken into account and this could be resolved by fast MoM design in this work.

The rest of the paper is organized in the following five sections. In Section II, a review of previous research on rapid analysis of the waveguide antenna by MoM is given, and the

The associate editor coordinating the review of this manuscript and approving it for publication was Kai-Da Xu.

© 2024 The Authors. This work is licensed under a Creative Commons Attribution 4.0 License.
For more information, see https://creativecommons.org/licenses/by/4.0/

innovation of the present work is highlighted. In Section III, the proposed antenna structure is illustrated, and its operation principle is explained. In Section IV, a comprehensive description of the design procedure of the feeding element array by fast MoM is given. Afterward, the manufactured antenna prototype is measured, and the results are discussed in Section V. Finally, a conclusion is provided in Section VI.

II. SURVEY ON PREVIOUS WORK AND INNOVATION OF THE PRESENT WORK

Plenty of work has been focusing on employing MoM for analyzing the waveguide slot array antenna to execute a rapid and efficient computation, either with a series-feed scheme [11], [17], [18] or a corporate-feed scheme [19], [20]. For instance, the CPU times are decreased to 50% in [11]. In [20], the radiating slot subarray is fast optimized by combining the MoM and the genetic algorithm, which shows excellent efficiency.

The MoM calculation for parallel-plate antennas usually make simplified assumptions which causes inaccuracy results especially when mutual coupling is strong. These assumptions are made in both the slot region [17], [21] and in the waveguide region for perturbation elements [22] or multilayer structure [23]. In [22], the structure consists of a radiating slot and a reflection-canceling post allocated in the waveguide is studied by MoM with simple current approximation on the post surface and checked by measurements. However, the discrepancy becomes non-negligible when the mutual coupling between the post and the slot is strong, which is common in slot array antenna designs. One way to guarantee accuracy is by applying more accurate models and analysis methods. For example, the round-edged effect of the slot is included by a hybrid FEM/MoM method in [24], while the rectangular slot with simple sinusoidal slot aperture field distribution is assumed in conventional MoM. However, complicated analysis would cause a rapid increase in the computation time and not suitable especially for the parameter optimization. Another choice is to introduce the equivalent parameters in the conventional MoM for compensating the inaccurate assumptions. In [25], the equivalent length for a rectangular slot is proposed for including the round-ended effect. In [23], a simplified double layer MoM analysis model with equivalent permittivity is applied for a RLSA design instead of the time-consuming full four-layer analysis. This method balances the calculation speed and accuracy and suitable for a fast design.

The above researchers deal with equivalent parameters in each region independently. However, this is not enough for the feeding structure design in this paper where several inaccurate assumptions are made for elements in different regions, and multiple equivalent parameters are needed for the analysis. All the equivalent parameters influence each other due to the mutual coupling and should be treated as a complete unit. As an innovation in this paper, a design parameter relationship between the HFSS and MoM models is introduced, which includes all the effects caused by inaccurate simplified approximations in MoM calculation simultaneously, and thus guarantee the calculation accuracy.

III. ANTENNA CONFIGURATION

The structure of the proposed antenna is illustrated in Fig. 1. The design frequency is $f_0 = 9.65$GHz. The antenna is composed of feeding part and radiating part. The feeding part consists of an antenna input, a τ junction, a waveguide feeder and coupling slots. The antenna input and the waveguide feeder are standard WR90 aluminum rectangular waveguide feeders with a wall thickness of 1mm. $2N$ coupling slots is located on the waveguide feeder to excite the radiating part, where $N = 15$. The radiating part is composed of parallel plates and radiation slot pairs. The parallel plates are filled by Nomex honeycomb core with peripheries shorted by aluminum frame. The radiating slot pairs for linear polarization are arrayed on the upper parallel plate.

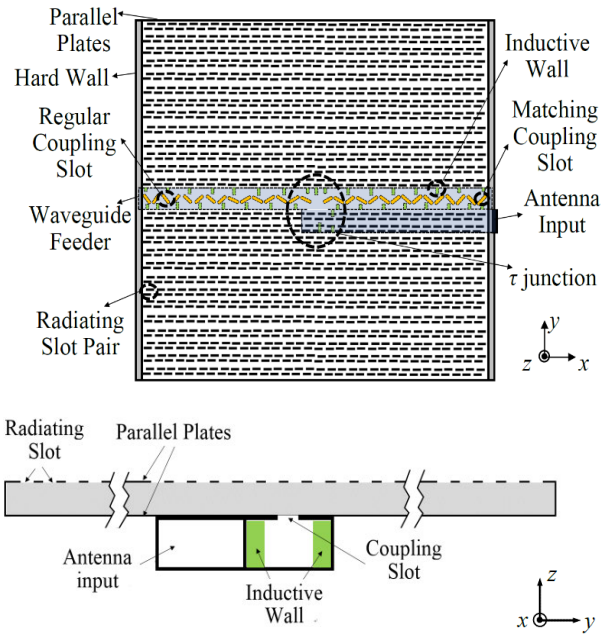

FIGURE 1. Antenna configuration, (a) top view, (b) layered structure.

A TE_{10}-mode from the antenna input travels in the -x direction. After it arrives the τ junction, the power is equally divided and propagates in both the $+x$ and $-x$ directions. The wave couples with the parallel plates through N inclined coupling slots on both sides of the τ junction and arranged along the center of the waveguide. Adjacent coupling slots are placed with opposite orientation and a spacing of approximately half guided wavelength $\lambda_g/2$ in order to feed the parallel plates in phase with uniform amplitude, where $\lambda_g = 42.4$mm denotes the guided wavelength in the feeder waveguide at f_0. Inductive walls are added for canceling the reflection. The coupled waves then propagate in both the $+y$ and $-y$ directions within parallel plates and radiate through radiating slot pairs. Two dielectric materials with 4.9mm thickness and relative permittivity $\varepsilon_{rh} = 3.6$ are placed at

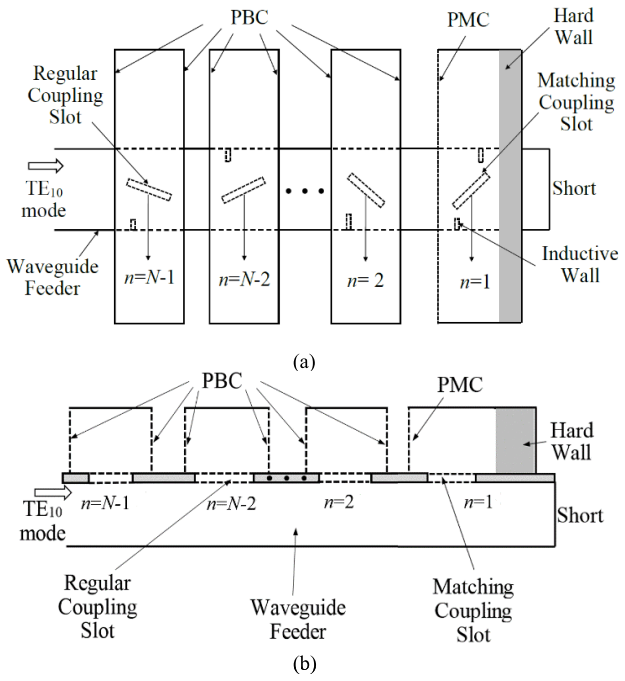

FIGURE 2. Analysis model of the waveguide feeder slot array, (a) top view, (b) side view.

edges of the parallel plates in order to increase aperture efficiency [26].

IV. DESIGN OF REGULAR ELEMENT ARRAY

In this section, coupling slots of a waveguide feeder in the 9.65GHz band is designed. The design model of the waveguide feeder slot array with (N-1) coupling slots is illustrated in Fig. 2 and the slot number n is counted from the shorted end. Parallel plates are modeled by waveguide array with periodic boundary condition (PBC) side walls for simplification. Coupling slot with width 2mm and inductive walls with the width 1mm are applied in the model. Only half part of the structure is shown due to the symmetry. The design aims to achieve minimum reflection in the waveguide and uniform field distribution in the parallel plate region. The coupling factor of the nth slot is required to be $1/n$ for exciting the parallel plate region uniformly. A design procedure of the coupling slots for the feeder network is given as follows.

A brief design process flowchart is given in Fig. 3. The design can be divided into two steps: (1) An initial design of individual coupling slots; (2) A further iterative optimization by the high-speed MoM analysis for the element array which includes the mutual coupling effect. The simplified assumptions employed in the MoM analysis would cause inaccuracies. Hence in step (1), various parameter equivalent relationship between the MoM and HFSS element models is found for the compensating. In step (2), the MoM designed parameters will be translated to the corresponding HFSS equivalent parameters as the actual fabrication parameters.

The following section would be divided into three parts. Part A is devoted to the basic principle of the MoM analysis of the slot array. Part B shows the individual slot design and explains the parameter equivalent relationship in detail. Some calculation results of the representative slots are given. Finally, the procedure of the element array design through iterative optimization is given in Part C.

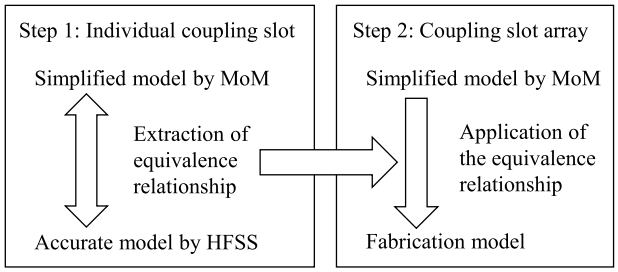

FIGURE 3. Design procedure flow chart for the feeder network.

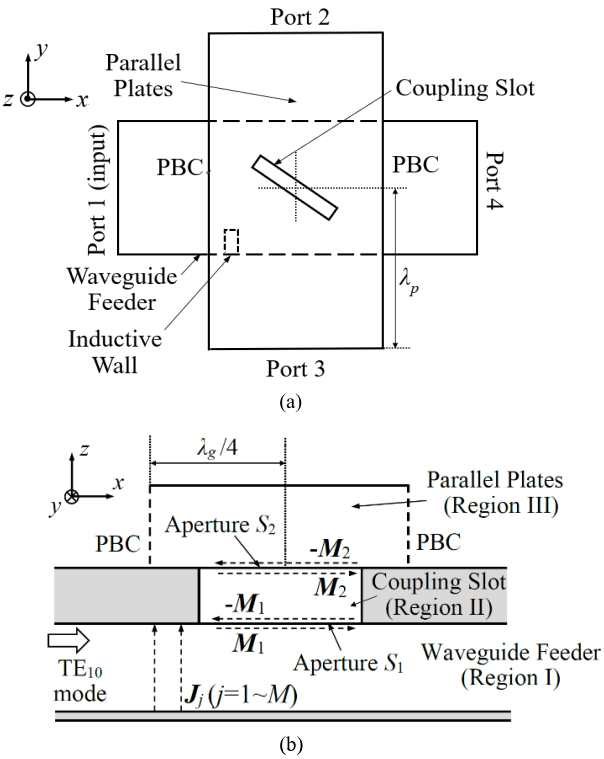

FIGURE 4. MoM analysis model for the coupling slot, (a) top view, (b) side view.

A. MOM ANALYSIS OF REGULAR ELEMENT ARRAY

Both the top and the side views of the MoM analysis model for a single coupling slot cut on feeder waveguide are shown in Fig. 4. External mutual coupling effect among the uniformly-excited coupling slots in the parallel plates region is included by introducing PBC in the side walls. Port 1 and Port 4 represent feeder input and output, respectively. Port 2 and Port 3 are outputs in parallel plate region.

Based on the field equivalence principle, both the bottom aperture S_1 and top aperture S_2 of coupling slots are replaced by unknown magnetic currents $\mathbf{M}_1$ and $\mathbf{M}_2$ backed with

perfect electric conducting sheet, while the inductive wall is replaced by unknown electric current along its surface. The magnetic current is expanded by P basis functions with sinusoidal distribution along the slot length, and the electric current is simplified by sets of M unknown uniform line currents $\mathbf{J}_q$ $(q = 1 \sim M)$ with only the z component, as shown follows,

$$\mathbf{M}_k = \sum_{j=1}^{P} V_{kj}\mathbf{m}_{kj} = \hat{u}\sum_{j=1}^{P} V_{kj}\sin\{\frac{j\pi}{l}(u+\frac{l}{2})\} \quad (k=1,2)$$
$$\mathbf{J}_q = I_q\mathbf{j}_q = \hat{z}I_q \quad (q = 1 \sim M) \tag{1}$$

where l represents the slot length, V_{kj} are complex weighting coefficients for $\mathbf{m}_{kj}$ on S_k, and I_q are complex amplitude for $\mathbf{J}_q$. The overall structure is divided to three canonical regions as shown in Fig. 4(b): waveguide feeder (an infinitely-long waveguide feeder) as Region I, coupling slot (a rectangular cavity) as Region II, and parallel plates region (a PBC waveguide) as Region III. Next, by imposing boundary conditions, i.e., the continuity of tangential magnetic field on the slot apertures (S_1 and S_2) as well as zero tangential electric field along the wall surface (S_w), coupled integral equations with respect to $\mathbf{M}_1$, $\mathbf{M}_2$ and $\mathbf{J}_q$ $(q = 1 \sim M)$ are derived. Then the application of Galerkin's MoM reduces integral equations to a system of linear equations for V_{kj} $(k = 1, 2)$ and I_q,

$$\begin{bmatrix} [Z_{pq}^{(\mathrm{I})}] & [M_{pj}^{(\mathrm{I})}] & [0] \\ [N_{iq}^{(\mathrm{I})}] & [Y_{ij}^{11(\mathrm{I})}]+[Y_{ij}^{11(\mathrm{II})}] & -[Y_{ij}^{12(\mathrm{II})}] \\ [0] & -[Y_{ij}^{21(\mathrm{II})}] & [Y_{ij}^{22(\mathrm{I})}]+[Y_{ij}^{22(\mathrm{III})}] \end{bmatrix} \cdot \begin{bmatrix} [I_q] \\ [V_{1j}] \\ [V_{2j}] \end{bmatrix} = \begin{bmatrix} -[e_q] \\ -[i_j] \\ [0] \end{bmatrix} \tag{2}$$

The reactions in (2) are expressed as,

$$\begin{aligned} Z_{pq}^{(1)} &= \int_{S_w} dS_o \mathbf{j}_p(\mathbf{r}_o) \int_{S_w} dS_s \overline{\mathbf{G}}_{ee}^{(1)}(\mathbf{r}_o,\mathbf{r}_s)\cdot\mathbf{j}_q(\mathbf{r}_s) \\ M_{pj}^{(1)} &= \int_{S_w} dS_o \mathbf{j}_p(\mathbf{r}_o) \int_{S_1} dS_s \overline{\mathbf{G}}_{em}^{(1)}(\mathbf{r}_o,\mathbf{r}_s)\cdot\mathbf{m}_j(\mathbf{r}_s) \\ N_{iq}^{(1)} &= \int_{S_1} dS_o \mathbf{m}_{1i}(\mathbf{r}_o) \int_{S_w} dS_s \overline{\mathbf{G}}_{me}^{(1)}(\mathbf{r}_o,\mathbf{r}_s)\cdot\mathbf{j}_q(\mathbf{r}_s) \\ Y_{ij}^{ab(r)} &= \int_{S_a} dS_o \mathbf{m}_{ai}(\mathbf{r}_o) \int_{S_b} dS_s \overline{\mathbf{G}}_{mm}^{(r)}(\mathbf{r}_o,\mathbf{r}_s)\cdot\mathbf{m}_{bj}(\mathbf{r}_s) \end{aligned} \tag{3}$$

where $\overline{\mathbf{G}}$ ' s represent the dyadic Green's functions are referred to as follows,

$\overline{\mathbf{G}}_{ee}^{(1)}(\mathbf{r}_o,\mathbf{r}_s)$: the electric field at $\mathbf{r}_o$ produced by a unit dyadic electric current source at $\mathbf{r}_s$ in Region I;

$\overline{\mathbf{G}}_{em}^{(1)}(\mathbf{r}_o,\mathbf{r}_s)$: the electric field at $\mathbf{r}_o$ produced by a unit dyadic magnetic current source at $\mathbf{r}_s$ in Region I;

$\overline{\mathbf{G}}_{me}^{(1)}(\mathbf{r}_o,\mathbf{r}_s)$: the magnetic field at $\mathbf{r}_o$ produced by a unit dyadic electric current source at $\mathbf{r}_s$ in Region I;

$\overline{\mathbf{G}}_{mm}^{(r)}(\mathbf{r}_o,\mathbf{r}_s)$: the magnetic field at $\mathbf{r}_o$ produced by a unit dyadic magnetic current source at $\mathbf{r}_s$ in Region $r(r$ = I, II or III);

e_q is the moment of one unit line electric current with the electric field of incident wave, and i_j is the moment of one basis function of the magnetic current with the magnetic field of incident wave. In (3), both a and b take 1 or 2. $i, j = 1, \ldots P$ represent the number of basis functions of magnetic currents on slot, while p, q = 1, 2, …, M represent the number of line currents on inductive walls. Reflection and coupling characterized by scattering matrix can then be obtained easily. Only one basis function is utilized ($P = 1$) in the calculation for reducing the computation time.

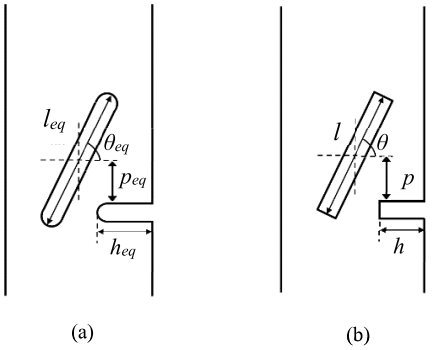

FIGURE 5. Definition of parameters in models for an individual slot, (a) equivalent parameter in HFSS model, (b) design parameter in MoM model.

B. INDIVIDUAL REGULAR COUPLING SLOT DESIGN AND EQUIVALENT RELATIONSHIP

The $n = 2 \sim N$-1 (N = 15) slot is called as a regular coupling element. Each element is initially designed by Fig. 4 with MoM described in Part A to control coupling and to suppress the reflection. The coupling is mainly affected by the slot angle while the reflection is controlled by the wall height and position. The reflection below -20dB is achieved for all the slots.

It should be noticed that simplified assumptions are used in MoM analysis to speed up the MoM analysis. This led to a difference in calculation results between the MoM and the actual model with the same design parameters. There are three simplifications: edge shapes, media in parallel plate region, current distribution on inductive wall. These simplifications can be compensated by a parameter translation. Various parameters of both the MoM and HFSS models for an individual slot are defined in Fig. 5, where all subscripts 'eq' in the HFSS model stands for the introduced equivalent parameters of the corresponding MoM parameters. The simplification in the MoM analysis and the parameter equivalent relationships are explained in detail as follows.

The first simplification is the media of the parallel plate region. For fabrication, the honeycomb core [27] is stabilized and bonded with the parallel plates by thin adhesive layers made of epoxy film with relative permittivity ε_{ra} = 3.08, i.e., the honeycomb layer is sandwiched by two adhesive sheets as a triple-layered structure in parallel plates, which is illustrated in Fig. 6 (a). The thickness of honeycomb core

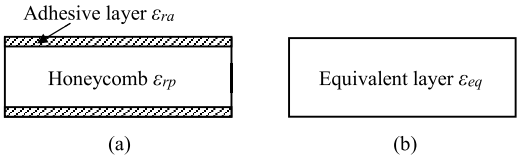

FIGURE 6. Cross-section of the parallel plates region, (a) HFSS model with triple layer, (b) MoM model with single layer.

and adhesive layer are represented by parameters $t_h = 6$mm and $t_a = 0.09$mm, respectively. If this triple layer structure applied in MoM analysis, the unknowns and computational complexity would be increased. However, it is possible to model the parallel plates region as single equivalent layer approximately due to the thickness of the adhesive layer is far less than that of the honeycomb core, as shown in Fig. 6 (b). It is aimed to compensate the multilayer effect in the HFSS model by introducing an equivalent permittivity ε_{eq} in the simplified MoM analysis. However, the aperture impedance presented to the input waveguide is under the influence of the permittivity in parallel plates region of the MoM model, which would further affect the coupling. This would cause a coupling difference between the MoM and HFSS models. The coupling could be mainly controlled by the slot angle. Therefore, a slot angle equivalent relationship is introduced for compensating the coupling difference.

The second simplification is the shape of the edges for the coupling slots and the inductive walls. In Part A, narrow rectangular slots and inductive walls with finite thickness are assumed in the MoM analysis for simplicity. In manufacturing, on the other hand, drilling process makes elements have semicircular ends and differ from the analysis model, which can be easily observed from Fig. 5 (a). Hence, there is a difference of the electrical field and current distribution near the semicircular region between the MoM and HFSS models, which consequently causes a different resonant frequency. The slot length and the wall height relationships are introduced for this round-edged effect.

The third simplification is electric current distribution of the inductive walls. The electric current along the wall surface is assumed to be uniform distributed in the MoM model while it is changed along the wall height because of the slot coupling. Moreover, only axial component is considered for the surface current, which is not accurate especially when the wall closes to the coupling slot. To cope with these current approximations in the MoM model, the wall position relationship is applied.

The HFSS equivalent parameters for an individual slot designed by MoM are found successively from $n = 2$ to $n = 14$. The equivalent relationships of slot angle, slot length, wall height and wall position are shown in Fig. 7. The trends of the data points are expected to behave linearly and four linear equations are used to estimate the linear behaviors, which are given as follows

$$\theta_{eq} = 1.00\theta + 1.12 \tag{4}$$

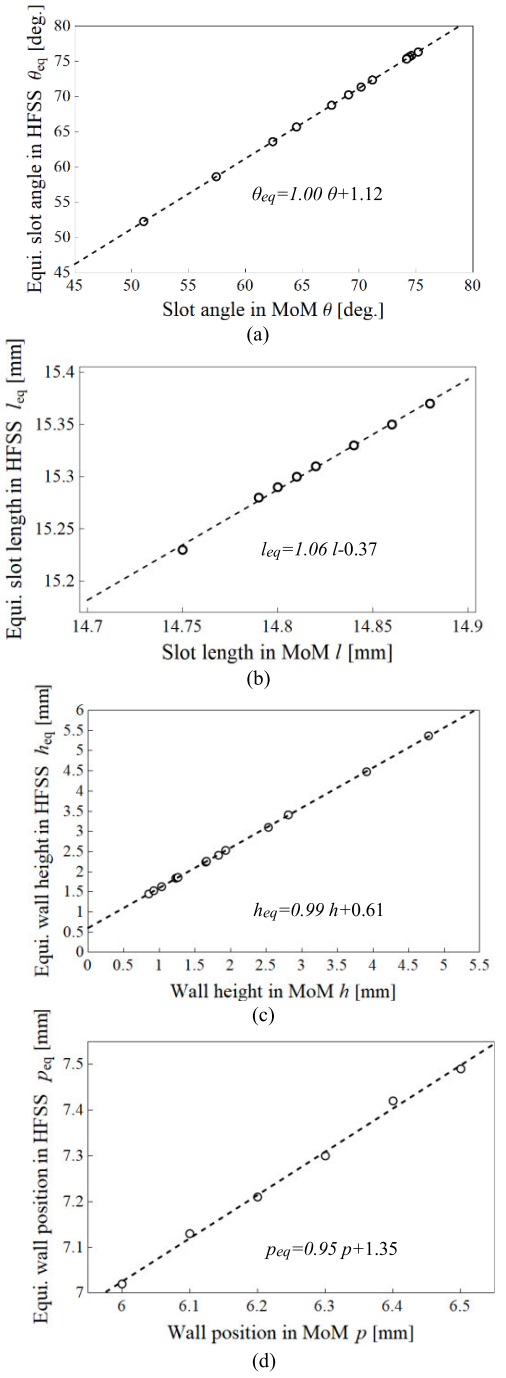

FIGURE 7. Equivalent relationship of the design parameters, (a) slot angle, (b) slot length, (c) wall height, (d) wall position.

$$l_{eq} = 1.06\, l - 0.37 \tag{5}$$

$$h_{eq} = 0.99\, h + 0.61 \tag{6}$$

$$l_{eq} = 0.95\, p + 1.35 \tag{7}$$

As an example, the calculation results by both the MoM and HFSS for the $n = 2, 5, 14$ slots are shown in Fig. 8. The resonant frequencies of the two models coincides and the coupling difference at 9.65GHz is less than 4%, which

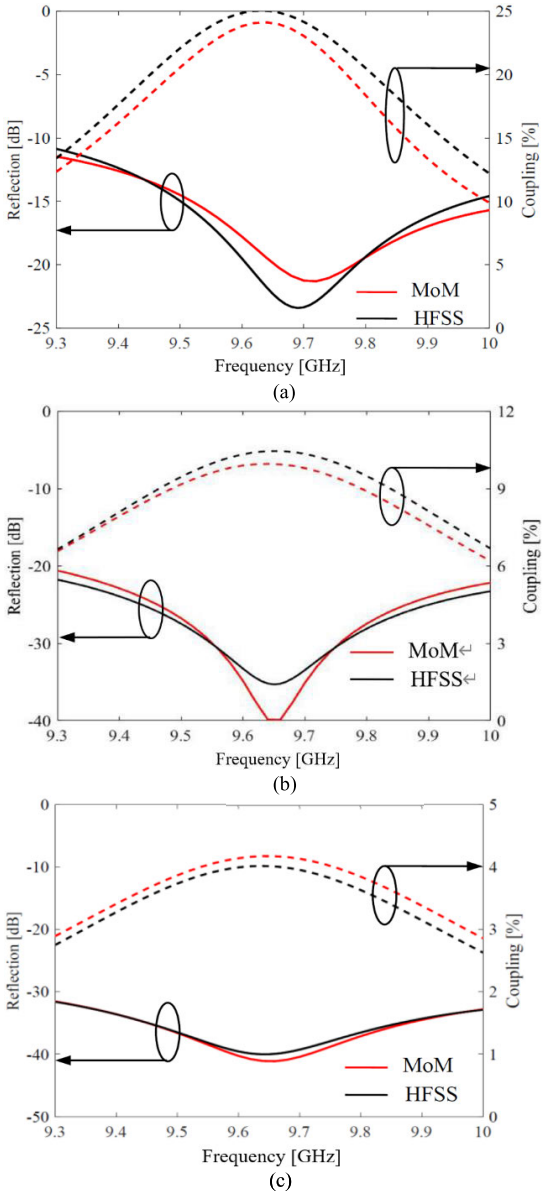

FIGURE 8. Calculation results of the single slot, (a) $n = 2$, (b) $n = 5$, (c) $n = 14$.

shows a good consistency between two calculation methods after introducing equivalent relationships. The laptop used for calculation has a 16-core Intel Core i7 CPU with 2.60GHz base frequency and 16GB RAM. The calculation time is 180 seconds by HFSS while it is 7 seconds by MoM which is much faster. The superiority of MoM on its calculation speed becomes important for the subsequent slot array design, which includes massive parameters.

C. REGULAR ELEMENT ARRAY DESIGN

Individual slot design only gives an initial design. Further slot array design by MoM is needed for including the effect of both the external mutual coupling in parallel plates region and the internal mutual coupling in waveguide feeder region. The analysis model is shown in Fig. 2. The external mutual

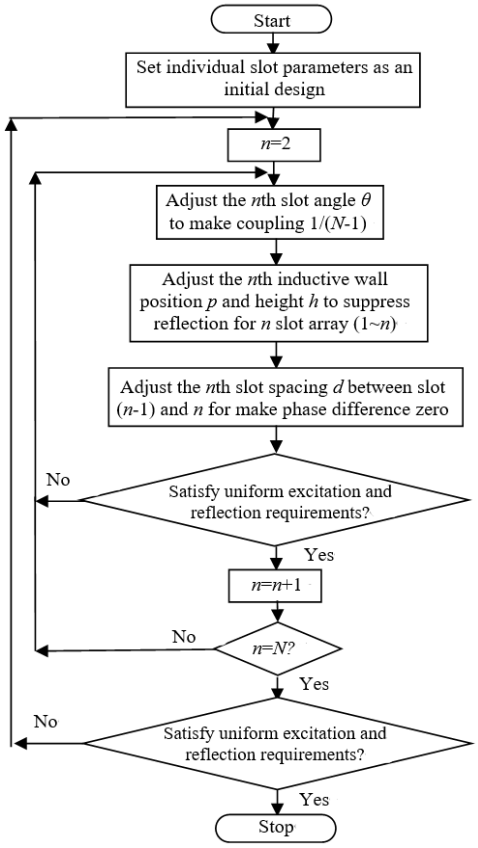

FIGURE 9. Flow chart of the slot array design iterative algorithm.

coupling among coupling slots is included by the employing PBC for radiating waveguide arrays. The MoM calculation follows the identical procedure explained in Part A. The internal mutual coupling within the feeding waveguide, i.e., the following reactions: (i) the reaction among electric currents along different inductive walls; (ii) the reaction among magnetic currents along different slot apertures; (iii) the reaction between electric currents and magnetic currents which corresponding to different walls and slots, are included in the reaction matrix of equation (2). For achieving a uniform field distribution, coupling to each radiating waveguide is expected to be $1/\{2(N\text{-}1)\} = 1/28 = 3.6\%$. To take the edge effect of into account, the matching slot ($n = 1$) is designed by HFSS [28] and the corresponding scattering parameters are cascaded to the regular slot array MoM code ($n = 2$-14).

An iterative design algorithm is presented, and Fig. 9 shows its flow chart. The slots are re-designed from $n = 2$ to $n = 14$ for suppressing the reflection level of the slot array, and for a uniform and in-phase excitation of parallel plates. It is worth noting that in this step, the fast-operating speed characteristic of MoM provides a possibility to this iterative progress. All the re-designed parameters for the slot array are then transformed to HFSS equivalent parameters for fabrication by using equations (4) - (7).

Fig. 10 gives the frequency characteristic of the reflection calculated by MoM and HFSS, which shows a similar

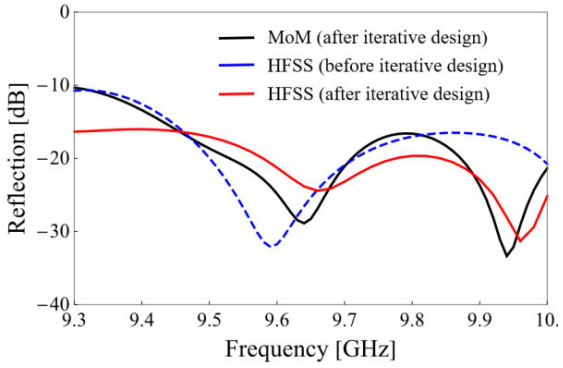

FIGURE 10. Reflection of the slot array.

tendency and resonant frequencies. The calculation results of coupling and transmission phase to the radiating waveguides are illustrated in Fig. 11. Without loss of generality, only the slots $n = 2$, 5, and 14 are given. It shows that the iterative algorithm improves the uniformity of the excitation. Among all slots, the coupling difference between MoM calculation and simulation is less than 2%, while the phase difference is less than 15 degrees after the iteration process, which guarantees a uniform feeding to the parallel plates. The small discrepancy between MoM and HFSS results demonstrates the validity of the introduced equivalent relationships. The calculation time of the element array by HFSS is about 4 hours while it is 20 seconds by MoM, which greatly reducing the time cost. However, it also indicates that the calculation errors of MoM and HFSS increase as the slot number n decreases, i.e., when the slot coupling factor increases. This is because a slot with a higher coupling factor leads to a stronger mutual coupling effect between electric currents flowing along the wall and induced currents along the slot aperture. Hence, a lower accuracy on the assumptions in MoM would be expected.

V. MEASUREMENT RESULTS OF FABRICATED ARRAY ANTENNA

A waveguide-fed antenna panel with 33 by 26 radiating elements was fabricated by machining and welding process as shown in Fig. 12. The feeding structure is composed of the regular coupling element array designed in the previous section and the matching coupling element presented in Appendix. The radiation part is the same as the previously designed one [28]. The fabricated antenna panel has a dimension of 687mm × 689mm. Near field and reflection measurement were conducted in an anechoic chamber.

A. NEAR FIELD MEASUREMENTS

The near field measurement setup is conducted in the anechoic chamber. The sampling step is set to be 15mm in both x and y directions. The measured and HFSS simulated one-dimensional E-field distributions at the design frequency of 9.65GHz, along the longitudinal direction and above the center of the panel (in the x direction, $y = 0$), are presented in Fig. 13. The dashed lines represent the corresponding linear

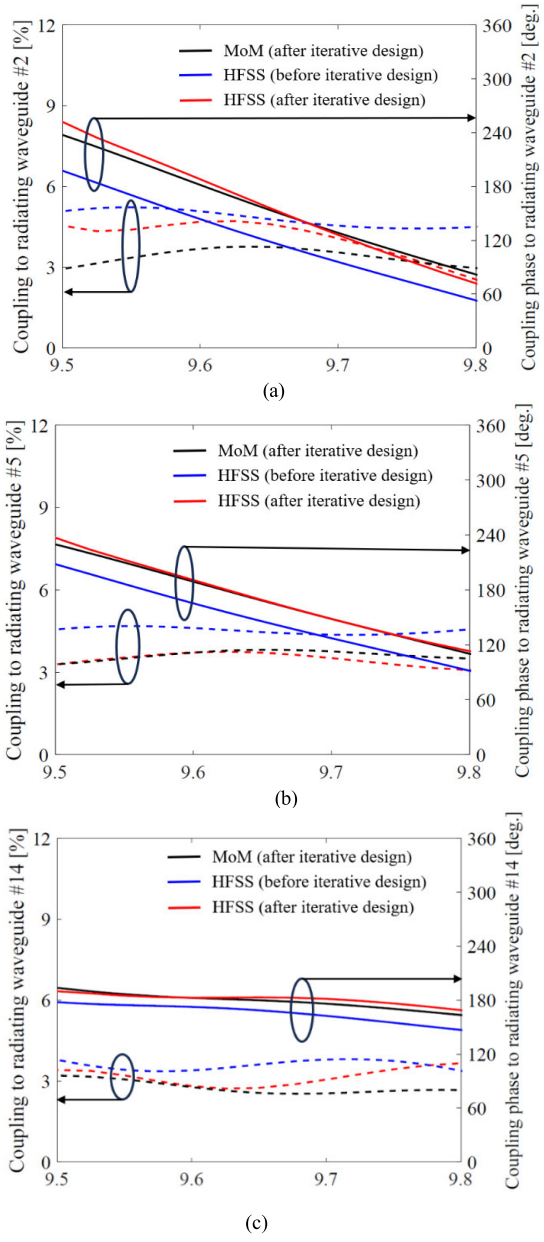

FIGURE 11. Calculation and simulation results of the coupling to radiating waveguides, (a) $n = 2$, (b) $n = 5$, (c) $n = 14$.

trendlines of amplitude and phase distributions calculated by the least squares method. The slopes are calculated as −1.1 dB/m and 23 deg./m, corresponding to the amplitude and phase distribution, respectively. The measured result shows a similar constant tendency to the simulated results, which confirm the operation of the feeder with uniform in-phase excitation. The measured amplitude and phase fluctuation level have deviations about 3-dB and 45-degree, respectively. These reasonable ripples are due to the wide spacing of adjacent coupling slots.

Radiation characteristics are calculated via the Fourier transform of the near field measurement data. Fig. 14 (a) shows the measured and HFSS simulated radiation patterns in the E-plane (y-$z$plane) and the H-plane (x-$z$plane) at 9.65GHz.

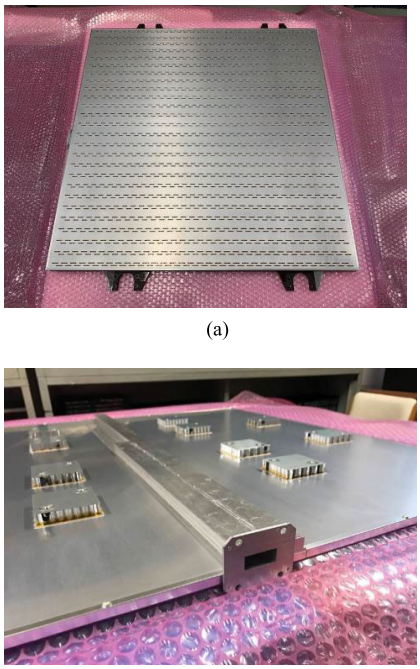

(a) (b)

FIGURE 12. Fabricated antenna panel, (a) overview, (b) waveguide feeder mount on the back side of the antenna panel.

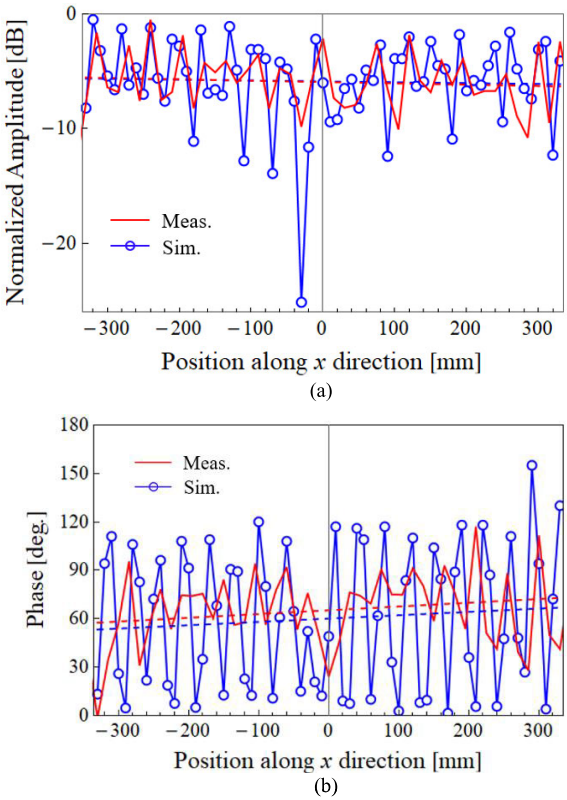

(a) (b)

FIGURE 13. 1-D E-field distributions along *x* direction @ 9.65GHz, (a) normalized amplitude, (b) phase.

A good agreement between the measurement and simulation in terms of the side lobes and the null positions can be

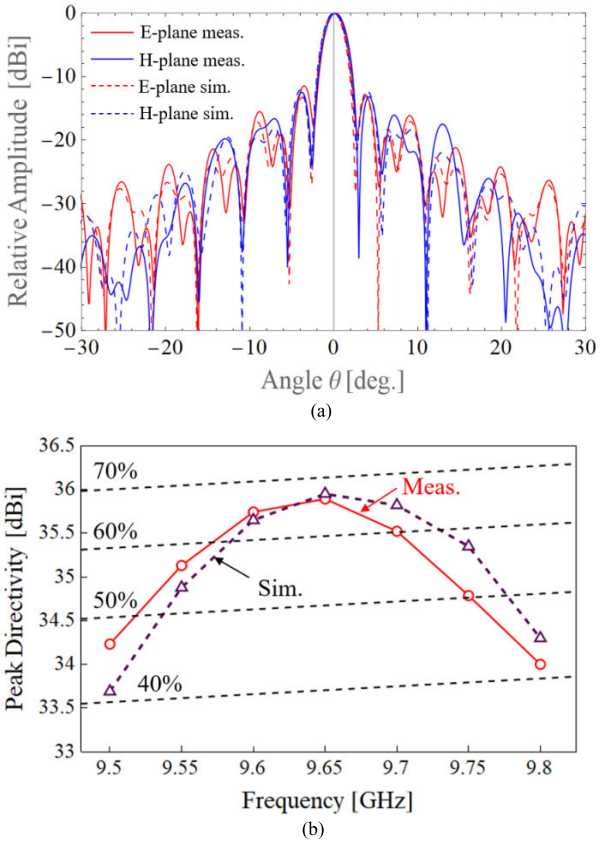

(a) (b)

FIGURE 14. Radiation characteristics of the antenna, (a) radiation patterns for E-plane and H-plane @ 9.65GHz, (b) peak directivity.

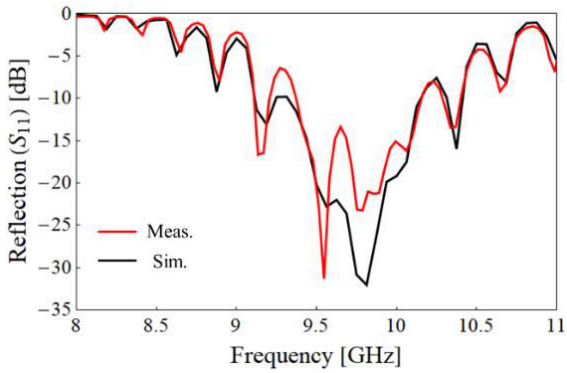

FIGURE 15. Frequency characteristics of the reflection.

observed. The 3dB-beamwidth is 2.4 degrees. The frequency behavior of the directivity is presented in Fig 14 (b). A maximum directivity at 9.65GHz with 36.0dBi and 67.7% aperture efficiency is demonstrated by measurement.

B. REFLECTION MEASUREMENTS

The reflection performance of the fabricated antenna is characterized by a vector network analyzer. The frequency dependance of the overall measured reflection are similar to the simulated results as shown in Fig. 15. Reflection below

TABLE 1. Performance comparison among related work on rectangular parallel-plate slot array antenna.

Ref.	Freq. [GHz]	Feed Scheme	Dimension $[\lambda_0 \times \lambda_0]^*$	No. of Elements	Peak Dir./Gain [dBi]	Peak Aperture Efficiency/ Antenna Efficiency [%]
[29]	59-64	Post-wall junctions	15.7×18.0	NA	NA/32.0	NA/47.4
[30]	11.5-12.5	Microstrip corporate network	11.2×14.4	24×20	28.8/NA	42.2/NA
[31]	74-78	Pillbox	13.4×12.7	29×23	27.4/>24	NA/>50
[32]	9.1-9.6	Dual reflector system	14.2×18.9	23×19	NA/NA	NA/81
[33]	48	Luneberg Lens	32×19.52	37	NA/30.4	NA/14
[34]	11.1-11.8	All-metal WG (Dielectric inserted)	15.35×14.39	26×18	NA/31.2	NA/48
[28]	9.5-9.8	All-metal WG	22.1 × 22.2	33×26	35.6/35.4	61.3/59.5
This work	9.5-9.8	All-metal WG	22.1 × 22.2	33×26	36.0/NA	67.7/NA

*: Here λ_0 denotes the free-space wavelength at the center frequency over the target bandwidth.

−10dB is confirmed from 9.38GHz to 10.38GHz according by measurement. At the design frequency, measured reflection is −13.38dB which is higher than the simulated one of −22.21dB. This discrepancy may be caused from the inaccuracy thickness of the manufactured adhesive layers, which apply to cover the honeycomb core. Moreover, the flatness of adhesive layers is not guaranteed in fabrication due to the effect of surface tension. One feasible way to compensate this reflection discrepancy is to change the lengths of the coupling slots.

C. PERFORMANCE COMPARISON

A performance comparison between this work and the related work on rectangular parallel-plate slot array antennas is given in Table 1. For exciting a quasi-TEM wave propagation in the oversized parallel-plate waveguide, feeding structures, including post-wall junctions [29] and microstrip corporate network [30], have been proposed. The feeding network is integrated with the radiating elements in the same layer, which facilitates the fabrication. However, the dielectric loss reduces the antenna efficiency. Various quasi-optical systems such as pillbox [31], dual reflector [32], or Lunenberg lens [33] have also been investigated to increase the field uniformity in parallel plates. However, such an excitation scheme needs additional space and makes the realization of high aperture efficiency difficult. In [28] and [34], and this work, a feeding waveguide placed beneath the parallel plates is employed as an alternative scheme of power distribution. The compact all-metal structure with no dielectric loss realizes a high efficiency. Compared to [28], this work enhances the performance by employing the fast MoM design with an internal mutual coupling effect included.

VI. CONCLUSION

In this paper, a waveguide feeder with reflection-canceling walls for a parallel-plate slot array antenna is analyzed and designed by Galerkin's MoM with design parameter relationship employed. This relationship between HFSS and MoM models is applied for compensating the inaccuracy in the MoM analysis. The fast calculation speed of the MoM enables an accurate array design which takes the mutual coupling effect into account. The designed waveguide feeder is fabricated and verified by measurements. A peak directivity of 36.0dBi and 67.7% aperture efficiency is achieved at 9.65GHz. A large discrepancy on reflection between measurement and simulation is observed. The possible reason is given as fabrication imperfections of the thin adhesive layers. One feasible way of to mitigate this reflection discrepancy is to change the lengths of the coupling slots and this would be verified as a future work.

REFERENCES

[1] J. Wu, Y. J. Cheng, and Y. Fan, "A wideband high-gain high-efficiency hybrid integrated plate array antenna for V-band inter-satellite links," *IEEE Trans. Antennas Propag.*, vol. 63, no. 4, pp. 1225–1233, Apr. 2015.

[2] V. Ravindra, P. R. Akbar, M. Zhang, J. Hirokawa, H. Saito, and A. Oyama, "A dual-polarization *X*-band traveling-wave antenna panel for small-satellite synthetic aperture radar," *IEEE Trans. Antennas Propag.*, vol. 65, no. 5, pp. 2144–2156, May 2017.

[3] S. Peng, C.-W. Yuan, T. Shu, J. Ju, and Q. Zhang, "Design of a concentric array radial line slot antenna for high-power microwave application," *IEEE Trans. Plasma Sci.*, vol. 43, no. 10, pp. 3527–3529, Oct. 2015.

[4] P. Kumar, A. Kedar, and A. K. Singh, "Design and development of low-cost low sidelobe level slotted waveguide antenna array in X-band," *IEEE Trans. Antennas Propag.*, vol. 63, no. 11, pp. 4723–4731, Nov. 2015.

[5] S. R. Rengarajan, M. S. Zawadzki, and R. E. Hodges, "Waveguide-slot array antenna designs for low-average-sidelobe specifications," *IEEE Antennas Propag. Mag.*, vol. 52, no. 6, pp. 89–98, Dec. 2010.

[6] M. Ando, Y. Tsunemitsu, M. Zhang, J. Hirokawa, and S. Fujii, "Reduction of long line effects in single-layer slotted waveguide arrays with an embedded partially corporate feed," *IEEE Trans. Antennas Propag.*, vol. 58, no. 7, pp. 2275–2280, Jul. 2010.

[7] M. Zhang, J. Hirokawa, M. Ando, Y. Tsunemitsu, and T. Taniguchi, "Design of a 39 GHz band alternating-phase fed double-layer waveguide slot antenna with the underneath partially-corporate feeding circuit," in *Proc. IEEE Int. Symp. Antennas Propag. (APSURSI)*, Jul. 2011, pp. 3033–3036.

[8] J. Liu, A. Vosoogh, A. U. Zaman, and J. Yang, "A slot array antenna with single-layered corporate-feed based on ridge gap waveguide in the 60 GHz band," *IEEE Trans. Antennas Propag.*, vol. 67, no. 3, pp. 1650–1658, Mar. 2019.

[9] N. Appannagarri, I. Bardi, R. Edlinger, J. Manges, M. Vogel, Z. Cendes, and J. Hadden, "Modeling phased array antennas in Ansoft HFSS," in *Proc. IEEE Int. Conf. Phased Array Syst. Techn.*, May 2000, pp. 323–326.

[10] K. Hashimoto and M. Higaki, "Practical design of radiating part of post-wall waveguide-fed parallel plate slot array antenna by method of moments," in *Proc. EuCAP*, Mar. 2020, pp. 1–5.

[11] E. Arnieri and G. Amendola, "Method of moments analysis of slotted substrate integrated waveguide arrays," *IEEE Trans. Antennas Propag.*, vol. 59, no. 4, pp. 1148–1154, Apr. 2011.
[12] M. Albani, G. La Cono, R. Gardelli, and A. Freni, "An efficient full-wave method of moments analysis for RLSA antennas," *IEEE Trans. Antennas Propag.*, vol. 54, no. 8, pp. 2326–2336, Aug. 2006.
[13] M. Kalfa and V. B. Ertürk, "Analysis of slotted sectoral waveguide arrays with multilayered radomes," *IEEE Trans. Antennas Propag.*, vol. 64, no. 2, pp. 800–805, Feb. 2016.
[14] M. Albani, A. Mazzinghi, and A. Freni, "Rigorous MoM analysis of finite conductivity effects in RLSA antennas," *IEEE Trans. Antennas Propag.*, vol. 59, no. 11, pp. 4023–4032, Nov. 2011.
[15] G. Mazzarella and G. Montisci, "Accurate modeling of coupling junctions in dielectric covered waveguide slot arrays," *Prog. Electromagn. Res. M*, vol. 17, pp. 59–71, 2011.
[16] P. R. Akbar, H. Saito, M. Zhang, J. Hirokawa, and M. Ando, "Parallel-plate slot array antenna for deployable SAR antenna onboard small satellite," *IEEE Trans. Antennas Propag.*, vol. 64, no. 5, pp. 1661–1671, May 2016.
[17] J.-H. Lee, T. Hirano, J. Hirokawa, and M. Ando, "Practical slot array design by method of moments using one basis function and constant correction length," *IEICE Trans. Commun.*, vols. E94–B, no. 1, pp. 158–165, Jan. 2011, doi: 10.1587/transcom.e94.b.158.
[18] T. Hirano, J. Hirokawa, and M. Ando, "Design of a waveguide crossed-slot array with matching elements using the method of moments with numerical-eigenmode basis functions," in *Proc. IEEE AP-S/URSI*, vol. 3, Jun. 2003, pp. 1046–1049.
[19] T. Tomura, J. Hirokawa, T. Hirano, and M. Ando, "A 45° linearly polarized hollow-waveguide 16 × 16-slot array antenna covering 71–86 GHz band," *IEEE Trans. Antennas Propag.*, vol. 62, no. 10, pp. 5061–5067, Oct. 2014.
[20] S. Ji, T. Tomura, and J. Hirokawa, "Fast analysis and bandwidth enhancement of the radiating subarray by method of moments for a parallel-plate slot array antenna with perpendicular-corporate feed," *IEEE Trans. Antennas Propag.*, vol. 70, no. 4, pp. 2645–2655, Apr. 2022.
[21] G. Montisci and G. Mazzarella, "Effect of the longitudinal component of the aperture electric field on the analysis of waveguide longitudinal slots," *IEEE Trans. Antennas Propag.*, vol. 59, no. 11, pp. 4334–4337, Nov. 2011.
[22] S. -H. Park, J. Hirokawa, and M. Ando, "Simple analysis of a slot and a reflection-canceling post in a rectangular waveguide using only the axial uniform currents on the post surface," *IEICE Trans. Commun.*, vol. E86-B, no. 8, pp. 2482–2487, Aug. 2003.
[23] T. X. Nguyen, S. J. Rushanthi, Y. Takano, K. Sakurai, T. Hirano, J. Hirokawa, M. Ando, O. Amano, S. Koreeda, and T. Matsuzaki, "An equivalent two-layer model for a fast design of a high gain multi-layer radial line slot antenna using MoM," in *Proc. Asia–Pacific Microw. Conf.*, Dec. 2012, pp. 595–597.
[24] M. Zhang, T. Hirano, J. Hirokawa, and M. Ando, "Analysis of a waveguide with a round-ended wide straight slot by the method of moments using numerical-eigenmode basis functions," *IEICE Trans. Commun.*, vol. E87-B, no. 8, pp. 2319–2326, Aug. 2004.
[25] H. Ueda, J. Hirokawa, M. Ando, O. Amano, and Y. Kamata, "A lightweight radial line slot antenna with honeycomb structure for space use," *IEICE Trans. Commun.*, vol. E91-B, no. 3, pp. 871–877, Mar. 2008.
[26] M. N. M. Kehn and P.-S. Kildal, "Miniaturized rectangular hard waveguides for use in multifrequency phased arrays," *IEEE Trans. Antennas Propag.*, vol. 53, no. 1, pp. 100–109, Jan. 2005.
[27] K. Miura and S. Pellegrino, *Forms and Concepts for Lightweight Structures*. New York, NY, USA: Cambridge Univ. Press, 2020, ch. 6.
[28] B. Pyne, P. R. Akbar, V. Ravindra, H. Saito, J. Hirokawa, and T. Fukami, "Slot-array antenna feeder network for space-borne *X*-band synthetic aperture radar," *IEEE Trans. Antennas Propag.*, vol. 66, no. 7, pp. 3463–3474, Jul. 2018.
[29] K. Hashimoto, J. Hirokawa, and M. Ando, "A post-wall waveguide center-feed parallel plate slot array antenna in the millimeter-wave band," *IEEE Trans. Antennas Propag.*, vol. 58, no. 11, pp. 3532–3538, Nov. 2010.
[30] M. Sierra-Casta ñer, M. Vera-Isasa, M. Sierra-Pérez, and J. L. Fernandez-Jambrina, "Double-beam parallel-plate slot antenna," *IEEE Trans. Antennas Propag.*, vol. 53, no. 3, pp. 977–984, Mar. 2005.
[31] M. Ettorre, R. Sauleau, L. Le Coq, and F. Bodereau, "Single-folded leaky-wave antennas for automotive radars at 77 GHz," *IEEE Antennas Wireless Propag. Lett.*, vol. 9, pp. 859–862, 2010.
[32] M. Ettorre, A. Neto, G. Gerini, and S. Maci, "Leaky-wave slot array antenna fed by a dual reflector system," *IEEE Trans. Antennas Propag.*, vol. 56, no. 10, pp. 3143–3149, Oct. 2008.
[33] K. Sato and H. Ujiie, "A plate Luneberg lens with the permittivity distribution controlled by hole density," *Electron. Commun. Jpn.*, vol. 85, no. 9, pp. 1–12, Sep. 2002.
[34] J. Hirokawa, M. Ando, and N. Goto, "Waveguide-fed parallel plate slot array antenna," *IEEE Trans. Antennas Propag.*, vol. 40, no. 2, pp. 218–223, Feb. 1992.

TIANYU WANG was born in Beijing, China, in 1994. He received the B.S. degree in automation science and electrical engineering from Beihang University, Beijing, in 2016, and the M.S. degree in electrical and electronic engineering from Tokyo University, Tokyo, Japan, in 2018. He is currently pursuing the Ph.D. degree in electrical and electronic engineering with Tokyo Institute of Technology, Tokyo.

His current research interests include electromagnetic wave analysis and slotted waveguide array antennas.

TAKASHI TOMURA (Member, IEEE) received the B.S., M.S., and D.E. degrees in electrical and electronic engineering from Tokyo Institute of Technology, Tokyo, Japan, in 2008, 2011, and 2014, respectively.

He was a Research Fellow with Japan Society for the Promotion of Science (JSPS), in 2013. From 2014 to 2017, he was with Mitsubishi Electric Corporation, Tokyo, engaged in research and development of aperture antennas for satellite communications and radar systems. From 2017 to 2019, he was a Specially Appointed Assistant Professor with Tokyo Institute of Technology, Tokyo, where he is currently an Assistant Professor. His research interests include electromagnetic analysis, aperture antennas, and planar waveguide slot array antennas. He received the Best Student Award from Ericsson, Japan, in 2012; the IEEE AP-S Tokyo Chapter Young Engineer Award, in 2015; and the Young Researcher Award from IEICE Technical Committee on Antennas And Propagation, in 2018.

JIRO HIROKAWA (Fellow, IEEE) was born in Tokyo, Japan, in 1965. He received the B.S., M.S., and D.E. degrees in electrical and electronic engineering from Tokyo Institute of Technology (Tokyo Tech), Tokyo, in 1988, 1990, and 1994, respectively.

He was a Research Associate (1990–1996) and an Associate Professor (1996–2015) with Tokyo Tech, where he is currently a Professor. He was with the Antenna Group, Chalmers University of Technology, Gothenburg, Sweden, as a Postdoctoral Fellow, from 1994 to 1995. He has authored or coauthored more than 200 peer-reviewed journal articles and more than 600 international conference presentations. His current research interests include analyses, designs, and fabrication techniques of slotted waveguide array antennas; millimeter-wave and terahertz antennas; and beam-switching circuits.

Dr. Hirokawa is a fellow of IEICE. He received the IEEE AP-S Tokyo Chapter Young Engineer Award, in 1991; the Young Engineer Award from IEICE, in 1996; Tokyo Tech Award for Challenging Research, in 2003; the Young Scientists' Prize from the Minister of Education, Cultures, Sports, Science and Technology, Japan, in 2005; the Best Paper Award (in 2007) and the Best Letter Award (in 2009) from IEICE Communications Society; and the IEICE Best Paper Award, in 2016 and 2018. He was the Chair of the Technical Program Committee for ISAP 2016; and the IEICE Technical Committee on Antennas and Propagation, from 2017 to 2019. He served as an Associate Editor for *IEICE Transactions on Communications* from 1999 to 2003 and from 2004 to 2007; IEEE TRANSACTIONS ON ANTENNAS AND PROPAGATIONS, from 2013 to 2016. He has been serving as a Track Editor for IEEE TRANSACTIONS ON ANTENNAS AND PROPAGATIONS, since 2016.